Journal of Chemical Engineering and Energy Materials (JCEEM)

Journal homepage: https://www.jceem.com/

DOI: 10.22034/jceem.2026.568308.1026

Optimized Photocatalytic Degradation of Ciprofloxacin Using a UV-C-Activated g-C_3N_4/Fe_3O_4 Heterostructure via Response Surface Methodology

Mohammad Moein Mehrdadian[1*], Masoud Parsania[2]

[1]PhD Candidate in Chemical Engineering, Kurdistan University, Sanandaj, Iran

[2]MSc in Chemistry, Razi University, Kermanshah, Iran

Article info

Received: 23.12.2025

Accepted: 19.02.2026

Available Online: 19.02.2026

Checked for Plagiarism: Yes

Keywords:

g-C_3N_4/Fe_3O_4, Ciprofloxacin, UV-C Photocatalysis, Response Surface Methodology, Central Composite Design, COD Removal

A B S T R A C T

Ciprofloxacin is a widely detected fluoroquinolone antibiotic whose high chemical stability and low biodegradability contribute to its persistence in aquatic environments. In this study, a magnetically recoverable g-C_3N_4/Fe_3O_4 heterostructured nanocomposite was investigated as a UV-C-activated photocatalyst for aqueous ciprofloxacin degradation. To elucidate the governing process parameters and optimize photocatalytic performance, the effects of initial ciprofloxacin concentration (5–120 mgL^{-1}), catalyst dosage (0.05–0.25 gL^{-1}), and solution pH (4–10) were systematically evaluated using a central composite design in conjunction with response surface methodology. Photocatalytic experiments were conducted under UV-C irradiation (254 nm) with lamp powers of 10, 20, and 40 W. The experimental results were well described by quadratic models, with coefficients of determination (R^2) of 0.8371, 0.8372, and 0.882 for the three irradiation systems, respectively. Analysis of variance confirmed the statistical significance of the fitted models and demonstrated non-significant lack-of-fit ($p > 0.05$). Among the investigated variables, catalyst dosage and solution pH had the strongest effect on photocatalytic performance, whereas excessive initial ciprofloxacin concentrations negatively impacted mineralization efficiency due to photon attenuation and inner-filter effects. Numerical optimization indicated that maximum COD removal was achieved at an initial ciprofloxacin concentration of approximately 8.05 mgL^{-1}, a catalyst dosage of 0.23 gL^{-1} g-C_3N_4/Fe_3O_4, and near-neutral pH. Under these optimized conditions, COD removal efficiencies of 82.3%, 90.8%, and 98.6% were obtained for the 10, 20, and 40 W UV-C systems, respectively, in close agreement with experimental validation. The observed enhancement in photocatalytic activity is primarily attributed to improved charge carrier separation at the g-C_3N_4/Fe_3O_4 interface and more efficient utilization of incident UV-C photons. Overall, these findings highlight the potential of magnetically separable g-C_3N_4/Fe_3O_4 for the removal of persistent pharmaceutical contaminants and demonstrate the effectiveness of RSM as a practical tool for process optimization prior to scale-up.

Corresponding Author: **Mohammad Moein Mehrdadian (moeinmehrdadian@gmail.com- ORCID: 0000-0001-5456-8388)*

[2]Email: (parsaniamasoud@gmail.com- ORCID: 0009-0002-5092-6947)

Introduction

The continuous release of pharmaceutical residues into aquatic environments has become a critical environmental issue, primarily due to their persistence, biological activity, and insufficient removal by conventional wastewater treatment processes [1,2]. Among the various classes of pharmaceuticals, fluoroquinolone antibiotics and particularly ciprofloxacin (CIP), are consistently reported in municipal wastewater, hospital effluents, and surface waters worldwide. This widespread occurrence is largely attributed to the extensive clinical use of CIP and its inherent resistance to biodegradation [3]. Even at low concentrations, CIP has been shown to induce ecotoxicological effects, interfere with microbial ecosystems, and contribute to the development of antimicrobial resistance, underscoring the necessity for more effective treatment strategies [4, 5].

The limited removal of ciprofloxacin in conventional activated sludge systems can be primarily ascribed to its high chemical stability and poor biodegradability [4]. As a result, increasing research attention has been directed toward advanced treatment technologies that are capable of achieving complete mineralization rather than merely transforming the parent compound into potentially persistent by-products [6]. In this context, advanced oxidation processes (AOPs) have emerged as a particularly attractive option because they rely on the in-situ generation of highly reactive oxygen species (ROS), such as hydroxyl (·OH) and superoxide ($\cdot O_2^-$) radicals, which can non-selectively oxidize recalcitrant organic contaminants [7].

Among AOP-based techniques, heterogeneous photocatalysis has been widely investigated for the degradation of persistent pharmaceutical pollutants through light-induced redox reactions. However, commonly used photocatalysts such as TiO_2 and ZnO suffer from intrinsic limitations, including restricted spectral response, rapid recombination of photogenerated charge carriers, and low quantum efficiency under practical operating conditions [8]. In recent years, graphitic carbon nitride (g-C_3N_4) has attracted considerable interest as a metal-free semiconductor owing to its favorable band structure, chemical stability, and potential for visible-light-driven photocatalysis [9,10]. Despite these advantages, the photocatalytic performance of pristine g-C_3N_4 remains constrained by fast electron hole recombination and a relatively low specific surface area.

To address these limitations, coupling g-C_3N_4 with magnetic iron oxide (Fe_3O_4) nanoparticles has been proposed as an effective strategy. The incorporation of Fe_3O_4 can promote interfacial charge transfer, suppress recombination of charge carriers, and simultaneously enable rapid magnetic separation of the photocatalyst after treatment, thereby improving both catalytic efficiency and practical applicability [11,12].

On this basis, the present study focuses on: (I) the synthesis and characterization of a magnetically recoverable g-C_3N_4/Fe_3O_4 nanocomposite, (II) the systematic evaluation of its photocatalytic performance for ciprofloxacin degradation under UV-C irradiation, and (III) the optimization of key operational parameters using response surface methodology (RSM) to determine conditions leading to maximum COD (chemical oxygen demand) removal.

Literature Review

The environmental occurrence and persistence of antibiotics, particularly fluoroquinolones, have been widely reported in recent years. Among them, ciprofloxacin is frequently detected in wastewater effluents and surface waters and is regarded as a compound of significant ecological concern due to its chemical recalcitrance and biological activity [1-3]. Because conventional wastewater treatment systems are often unable to achieve complete ciprofloxacin removal, increasing attention has been directed toward advanced treatment strategies capable of promoting complete mineralization rather than partial transformation [4].

Photocatalytic advanced oxidation processes (AOPs) represent one of the most extensively studied approaches for antibiotic abatement, as they rely on the generation of ROS that can effectively degrade recalcitrant organic pollutants [6]. Early investigations predominantly focused on metal oxide photocatalysts such as TiO_2 and ZnO; however, practical limitations related to restricted spectral response, rapid charge carrier recombination, and narrow operational pH windows have motivated the exploration of alternative semiconductor materials [9].

In this context, graphitic carbon nitride (g-C_3N_4) has gained increasing interest as a metal-free photocatalyst with favorable chemical stability and visible-light responsiveness [13]. Nevertheless, its practical photocatalytic efficiency remains limited by fast electron–hole recombination. To overcome this drawback, hybridization with magnetic Fe_3O_4 nanoparticles has been proposed, leading to the development of g-C_3N_4/Fe_3O_4 heterostructures. Such composites have been reported to exhibit improved charge separation, enhanced ROS generation, increased adsorption capacity, and convenient magnetic recovery after treatment [11, 14].

Recent studies have demonstrated that g-C_3N_4/Fe_3O_4-based photocatalysts are effective for the degradation of dyes, pharmaceuticals, and antibiotics under both UV and visible irradiation, often outperforming the individual components [15]. With respect to ciprofloxacin, g-C_3N_4-based binary and ternary systems incorporating metal oxides or plasmonic materials have shown enhanced degradation and mineralization efficiencies, which have been attributed to improved light harvesting, interfacial charge transfer, and suppressed electron–hole recombination [5,16].

Despite these advances, photocatalytic performance remains highly sensitive to operational parameters such as photon flux, catalyst loading, solution pH, and pollutant concentration. Statistical optimization tools, including RSM coupled with CCD, are therefore increasingly employed to quantify variable interactions and establish predictive models for COD and TOC (total organic carbon) removal [17-19]. However, substantial discrepancies in reported optimal conditions persist

across studies, photon fluence is often insufficiently described, and the assessment of transformation product toxicity is frequently neglected. Addressing these limitations through systematic optimization and mechanistic analysis is essential for advancing photocatalytic processes toward reliable scale-up and practical implementation.

Materials and Methods

Chemicals and Materials:

All chemicals used in this study were of analytical grade and were used as received without further purification. Ciprofloxacin hydrochloride ($C_{17}H_{18}FN_3O_3$, purity ≥98%) was purchased from Sigma-Aldrich (USA) (Fig. 1). Sodium hydroxide (NaOH) and hydrochloric acid (HCl), employed for pH adjustment during the photocatalytic experiments, were also obtained from Sigma-Aldrich. UV-C lamps with nominal power outputs of 10, 20, and 40 W (λ = 254 nm) were supplied by Philips (Germany) and served as irradiation sources throughout the study.

Graphitic carbon nitride (g-C_3N_4) was synthesized by thermal polymerization of melamine following a conventional procedure. Fe_3O_4 nanoparticles were prepared via a co-precipitation method based on previously reported protocols. The g-C_3N_4/Fe_3O_4 magnetic nanocomposite was subsequently synthesized using a solid-state coupling strategy, with a post-calcination step applied to facilitate intimate interfacial contact, thereby promoting heterojunction formation between the two components. All synthesis procedures were carried out under carefully controlled conditions to ensure consistency and reproducibility.

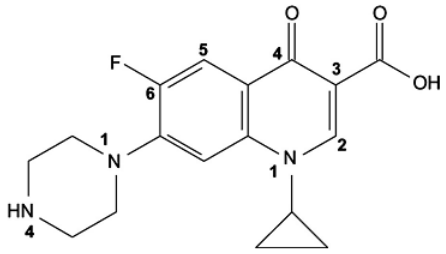

Fig. 1. Chemical structure of ciprofloxacin

Characterization:

The morphology and microstructural characteristics of the g-C_3N_4/Fe_3O_4 nanocomposite were examined using scanning electron microscopy (SEM, Hitachi S-4160). The crystalline structure and phase composition were analyzed using X-ray diffraction (XRD) on a Philips X'Pert PW 3040/60 diffractometer equipped with Cu Kα radiation (λ = 1.5406 Å). XRD measurements were performed to identify the characteristic diffraction peaks of g-C_3N_4 and Fe_3O_4 and to confirm the successful formation of the composite material. Representative SEM micrographs and XRD patterns of the synthesized nanocomposite are shown in Fig. 2.

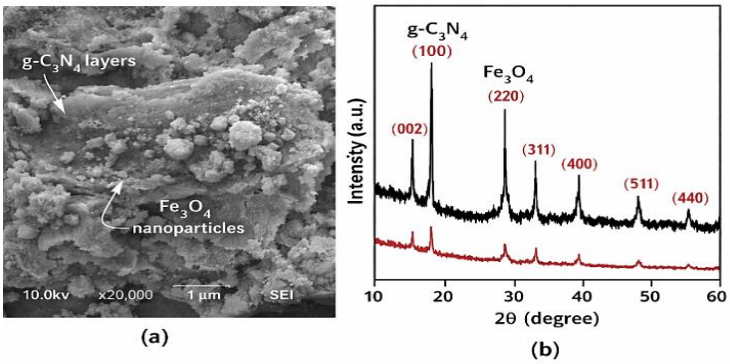

Fig. 2. (a) SEM image illustrating the morphology and microstructural features of the g-C_3N_4/Fe_3O_4 nanocomposite and (b) XRD pattern confirming its crystalline structure and phase composition.

Experimental Design and Optimization:

Process optimization was performed using RSM combined with a CCD to systematically evaluate both the individual and interactive effects of key operating parameters on photocatalytic performance. Based on preliminary experiments and relevant literature, three independent variables were selected: initial ciprofloxacin concentration (A, 5-120 mgL^{-1}), catalyst dosage (B, 0.05-0.25 gL^{-1} of g-C_3N_4/Fe_3O_4), and solution pH (C, 4-10).

The CCD matrix consisted of 20 experimental runs, including factorial points, axial points, and replicated center points, and was constructed according to standard RSM design principles. COD removal efficiency was chosen as the response variable (Y) to reflect the extent of mineralization achieved during the photocatalytic process. The experimental results were subsequently fitted to a second-order polynomial model, as expressed in Eq. (1):

$$Y = \beta_0 + \sum_{j=1}^{K} \beta_j x_i + \sum_{j=1}^{K} \beta_{jj} x_j^2 + \sum \sum_{i<j=2}^{K} \beta_{ij} x_i x_j \quad (1)$$

Where:

Where Y is the response variable (COD removal efficiency), x_i and x_j denote the coded independent variables, β_0 is the intercept, β_i is the linear coefficient, β_{ij} is the interaction coefficient, β_{ii} is the quadratic coefficient, and K is the number of independent variables (K = 3).

Batch Photocatalytic Experiments:

Photocatalytic degradation experiments were performed in a custom-built batch reactor fabricated from UV-transparent Plexiglas. The reactor consisted of a cylindrical reaction chamber with an effective working volume of 500 mL. To ensure stable thermal conditions during irradiation, the main chamber was surrounded by a secondary water-jacketed compartment (3 L capacity) connected to a recirculating water bath, maintaining the reaction temperature at 27 ± 2 °C.

UV-C irradiation was provided by vertically mounted low-pressure mercury lamps with nominal power outputs of 10, 20, and 40 W (λ = 254 nm). To enhance photon utilization within the reactor, all internal surfaces were lined with aluminum foil to promote light reflection. Continuous agitation was provided by a magnetic stirrer throughout the experiments to minimize external mass-transfer limitations during the photocatalytic process.

All photocatalytic experiments were performed according to the 20-run central composite design described in the previous section. Each batch experiment was conducted for 60 min, and all experimental conditions were repeated in triplicate to ensure reproducibility.

A fresh ciprofloxacin stock solution was prepared daily using deionized water and stored at 4 °C in the dark. The desired initial concentrations were obtained by appropriate dilution of the stock solution prior to each run. For each experimental run, the required volume of ciprofloxacin solution and the prescribed amount of g-C_3N_4/Fe_3O_4 nanocomposite were introduced into the reactor, and the solution pH was adjusted using standardized 1.0 M NaOH or 1.0 M HCl solutions. Before initiating UV-C irradiation, the suspension was magnetically stirred in the dark for 30 min to establish adsorption–desorption equilibrium between ciprofloxacin and the photocatalyst surface.

At the end of the irradiation period, the photocatalyst was rapidly separated from the treated solution by magnetic decantation and, when necessary, further assisted by centrifugation at 3000 rpm for 10 min. The collected supernatant was subsequently filtered through a 0.22 µm PTFE syringe filter (Schleicher & Schuell, Germany) to remove any remaining suspended particles. COD was determined using a HACH DR-5000 UV–Vis spectrophotometer following Standard Method 5220D (APHA, 2005). The COD removal efficiency (Y, %) was calculated according to Eq. (2):

$$Y(\%) = \frac{C_0 - C_e}{C_0} \times 100 \quad (2)$$

Where:

C_0 and C_e are initial and final COD concentrations.

Statistical Analysis:

The experimental data were analyzed using RSM via multiple regression modeling implemented in Design-Expert software (version 7.0). The adequacy of the fitted second-order polynomial models was evaluated by analysis of variance (ANOVA), including Fisher's F-test, lack-of-fit assessment, and significance testing of individual model coefficients. Statistical significance was defined at a 95% confidence level ($p < 0.05$).

The predictive performance and reliability of the developed models were further evaluated using the coefficient of determination (R^2), adjusted R^2, predicted R^2, and adequate precision. These statistical indicators were used to verify the robustness of the regression models and ensure that the RSM provided reliable predictions within the studied experimental domain.

Results

Model Fitting and Statistical Analysis:

The experimental and predicted COD removal efficiencies for the 20 experimental runs used to develop the regression models are summarized in Table 2. To account for differences in photon flux, separate CCD-based RSM models were developed for each UV-C lamp power, thereby enabling evaluation of the effects of operating parameters on COD removal efficiency under varying irradiation intensities.

Several regression models were examined, and a second-order polynomial model was identified as the most appropriate for predicting COD removal efficiency as a function of ciprofloxacin concentration (A), g-C_3N_4/Fe_3O_4 dosage (B), and solution pH (C). The model incorporates linear (A, B, C), interaction (AB, AC, BC), and quadratic (A^2, B^2, C^2) terms.

Model adequacy and predictive performance were evaluated using the coefficient of determination (R^2), adjusted R^2, predicted R^2, F-values, and lack-of-fit tests. The R^2 values were 0.8371, 0.8372, and 0.882 for the 10, 20, and 40 W systems, respectively, with close agreement between adjusted and predicted R^2 values, indicating satisfactory predictive reliability. In all cases, lack-of-fit p-values exceeded 0.05, confirming the statistical validity of the models. The corresponding F-values were 5.71, 5.71, and 8.31, with p-values of 0.0059, 0.0059, and 0.0014, demonstrating the statistical significance of the regression models (Tables 3-5).

Model coefficients were estimated using multiple regression analysis, and the resulting second-order polynomial equations including only statistically significant terms ($p < 0.05$) are presented in Eqs. (3-5). The close agreement between experimental and predicted COD removal efficiencies across all experimental runs confirms that the developed models adequately describe the photocatalytic behavior of the g-C_3N_4/Fe_3O_4 nanocomposite under UV-C irradiation.

$$\text{COD removal (\%)Lamp 10 W} = -287.02812 + 0.40034\,A + 686.54931\,B + 65.39452\,C - 1.68480\,AB - 0.061372\,BC - 40.18347\,AC + 3.56045E-004\,A^2 - 588.83278\,B^2 - 3.78574\,C^2 \quad (3)$$

$$\text{COD removal (\%)Lamp 20 W} = -275.39703 + 0.43958\,A + 772.28593\,B + 67.95696\,C - 1.63022\,AB - 0.081434\,BC - 56.13641\,AC + 1.45771E-003\,A^2 + 140.55322\,B^2 - 3.32490\,C^2 \quad (4)$$

$$\text{COD removal (\%)Lamp 40 W} = -278.37775 + 0.31643\,A + 693.83654\,B + 68.30807\,C - 1.03450\,AB - 0.044972\,BC - 56.61898\,AC - 4.66350E-004\,A^2 + 206.47064\,B^2 - 3.64937\,C^2 \quad (5)$$

Table 2. Central composite design (CCD) and observed responses

Run Order	Actual Variables			COD Removal (%)					
				Experimental			Predicted		
	Factor 1: CIP concentration (mg L^{-1})	Factor 2: g-C_3N_4/Fe_3O_4 dosage (g L^{-1})	Factor 3: solution pH	Lamp 10 W	Lamp 20 W	Lamp 40 W	Lamp 10 W	Lamp 20 W	Lamp 40 W
1	62.50	0.16	4.00	3.4	7.2	11.8	2.13	6.91	13.42
2	28.30	0.09	5.60	8.8	9.5	17.7	18.77	19.15	25.82
3	28.30	0.21	5.60	47.8	53.5	68.1	54.83	59.89	71.31
4	96.70	0.09	5.60	19.2	23.3	23.2	15.16	19.60	19.57
5	96.70	0.21	5.60	48.1	58.2	69.3	38.83	47.54	57.20
6	5.00	0.16	7.00	82.2	85.2	87.1	65.54	68.42	73.41
7	62.50	0.05	7.00	25.6	32.5	37.1	20.71	26.75	31.40
8	62.50	0.16	7.00	46.9	51.2	62.9	50.14	50.97	62.11
9	62.50	0.16	7.00	45.6	60.3	69.2	50.14	50.97	62.11
10	62.50	0.16	7.00	45.3	48.8	59.8	50.14	50.97	62.11
11	62.50	0.16	7.00	58.2	45.8	55.7	50.14	50.97	62.11
12	62.50	0.16	7.00	48.6	52.7	67.1	50.14	50.97	62.11
13	62.50	0.16	7.00	56.7	47.2	57.1	50.14	50.97	62.11
14	62.50	0.25	7.00	59.4	68.3	83.6	63.21	72.84	90.36
15	120.00	0.16	7.00	21.7	27.8	32.8	37.09	43.16	47.73
16	28.30	0.09	8.80	38.6	44.2	48.7	44.09	50.86	55.06
17	28.30	0.21	8.80	59.6	65.3	75.8	65.85	71.64	80.24
18	96.70	0.09	8.80	29.1	35.1	40.1	27.04	33.49	38.96
19	96.70	0.21	8.80	46.2	50.5	65.4	36.42	41.47	56.46
20	62.50	0.16	10.00	29.5	36.1	46.1	30.01	35.18	45.12

Effect of Various Parameters on COD Removal:

The ANOVA results for the 10, 20, and 40 W UV-C lamps are summarized in Tables 3-5, respectively. Contour plots were employed to visualize the interactions between two independent variables while maintaining the third variable at its central level, thereby facilitating a clearer interpretation of parameter interdependencies.

Effect of CIP Concentration: Figure 3 illustrates the combined influence of ciprofloxacin concentration and g-C_3N_4/Fe_3O_4 dosage at pH 7. COD removal efficiency increased with increasing CIP concentration up to approximately 72 mgL^{-1}. Beyond this concentration, a plateau was observed, which can be attributed to saturation of active sites on the catalyst surface and limited photon availability to sustain further photocatalytic reactions.

Effect of g-C_3N_4/Fe_3O Dosage: Increasing the catalyst dosage enhanced COD removal efficiency until an optimum value of 0.23 gL^{-1} was reached. Further increases in catalyst loading resulted in a decline in removal efficiency, primarily due to increased light scattering and shielding effects, which reduced effective photon penetration and limited uniform irradiation of the catalyst surface.

Effect of Solution pH: The photocatalytic performance was highly dependent on solution pH (Figs 4-5). Maximum COD removal was achieved within the pH range of 5-9, with an optimum near pH ~7. This behavior can be attributed to the surface charge of g-C_3N_4/Fe_3O_4 and the acid–base behavior of ciprofloxacin, affecting adsorption and photocatalytic degradation.

Figure 5 further highlights the interactive effect of catalyst dosage and solution pH on COD removal efficiency, indicating that optimal performance results from a balance between catalyst loading and solution conditions.

Model Validation: Numerical optimization using the desirability function predicted maximum COD removal efficiencies of 82.3%, 90.8%, and 98.5% for the 10, 20, and 40 W UV-C lamps, respectively, at a CIP concentration of 8.05 mg L^{-1}, catalyst dosage of 0.23 gL^{-1}, and pH~7.18. Experimental validation under these conditions yielded COD removal efficiencies of 82.2%, 85.2%, and 87.1%, respectively.

Despite the larger deviation observed for the 40 W system, experimental trends generally followed the predicted values, confirming the practical reliability of the developed models (Table 6). The observed deviation at higher lamp power may be attributed to localized heating or non-uniform light distribution, potentially affecting photon utilization efficiency.

Table 3. Analysis of variance (ANOVA) for the fitted second-order polynomial model of COD removal under UV-C irradiation (10 W lamp)

Source	Sum of squres	df	Mean squre	F value	P value	
Model	5855.55	9	650.62	5.71	0.0059	Significant
A-CIP concentration	822.39	1	822.39	7.22	0.0228	
B-Catalyst dosage	2010.43	1	2010.43	17.64	0.0018	
C-pH	969.11	1	969.11	8.5	0.0154	
AB	78.00	1	78.00	0.68	0.4274	
AC	90.78	1	90.78	0.80	0.3931	
BC	104.67	1	104.67	0.92	0.3605	
A^2	2.45	1	2.45	0.021	0.8864	
B^2	56.32	1	56.32	0.49	0.4981	
C^2	1944.19	1	1944.19	17.06	0.0020	
Residual	1139.75	10	113.97			
Lack of fit	974.88	5	197.98	5.91	0.0367	Significant
Pure error	164.87	5	32.97			
Cor. total	6995.30	19				
R-Squred =	*0.8371*	*Adj R-Squred =*	*0.6904*	*Pred. R-Sqred =*	*-0.0024*	

Table 4. Analysis of variance (ANOVA) for the fitted second-order polynomial model of COD removal under UV-C irradiation (20 W lamp)

Source	Sum of squres	df	Mean squre	F value	P value	
Model	5851.42	9	650.16	5.71	0.00590	Significant
A-CIP concentration	631.73	1	631.73	5.55	0.0402	
B-Catalyst dosage	2365.45	1	2365.45	20.79	0.0010	
C-pH	1063.57	1	1063.57	9.35	0.0121	
AB	83.31	1	83.31	0.73	0.4122	
AC	159.84	1	159.84	1.40	0.2633	
BC	204.27	1	204.27	1.80	0.2099	
A^2	41.03	1	41.03	0.36	0.5615	
B^2	3.21	1	3.21	0.028	0.8700	
C^2	1499.67	1	1499.67	13.18	0.0046	
Residual	1137.65	10	113.76			
Lack of fit	1001.91	5	200.38	7.38	0.0234	Significant
Pure error	135.74	5	27.15			
Cor. total	6989.07	19				
R-Squred =	*0.8372*	*Adj R-Squred =*	*0.6907*	*Pred. R-Sqred =*	*-0.0281*	

Table 5. Analysis of variance (ANOVA) for the fitted second-order polynomial model of COD removal under UV-C irradiation (40 W lamp)

Source	Sum of squres	df	Mean squre	F value	P value	
Model	7590.53	9	843.39	8.31	0.0014	Significant
A-CIP concentration	701.98	1	701.98	6.91	0.0252	
B-Catalyst dosage	3870.28	1	3870.28	38.12	0.0001	
C-pH	1306.24	1	1306.24	12.87	0.0050	
AB	31.41	1	31.41	0.31	0.5903	
AC	48.75	1	48.75	0.48	0.5041	
BC	207.80	1	207.80	2.05	0.1830	
A^2	4.20	1	4.20	0.041	0.8429	
B^2	6.92	1	6.92	0.068	0.7993	
C^2	1806.65	1	1806.65	17.80	0.0018	
Residual	1015.16	10	101.52			
Lack of fit	870.81	5	174.16	6.03	0.0353	Significant
Pure error	144.35	5	28.87			
Cor. total	8605.69	19				
R-Squred =	*0.8820*	*Adj R-Squred =*	*0.7759*	*Pred. R-Sqred =*	*0.2661*	

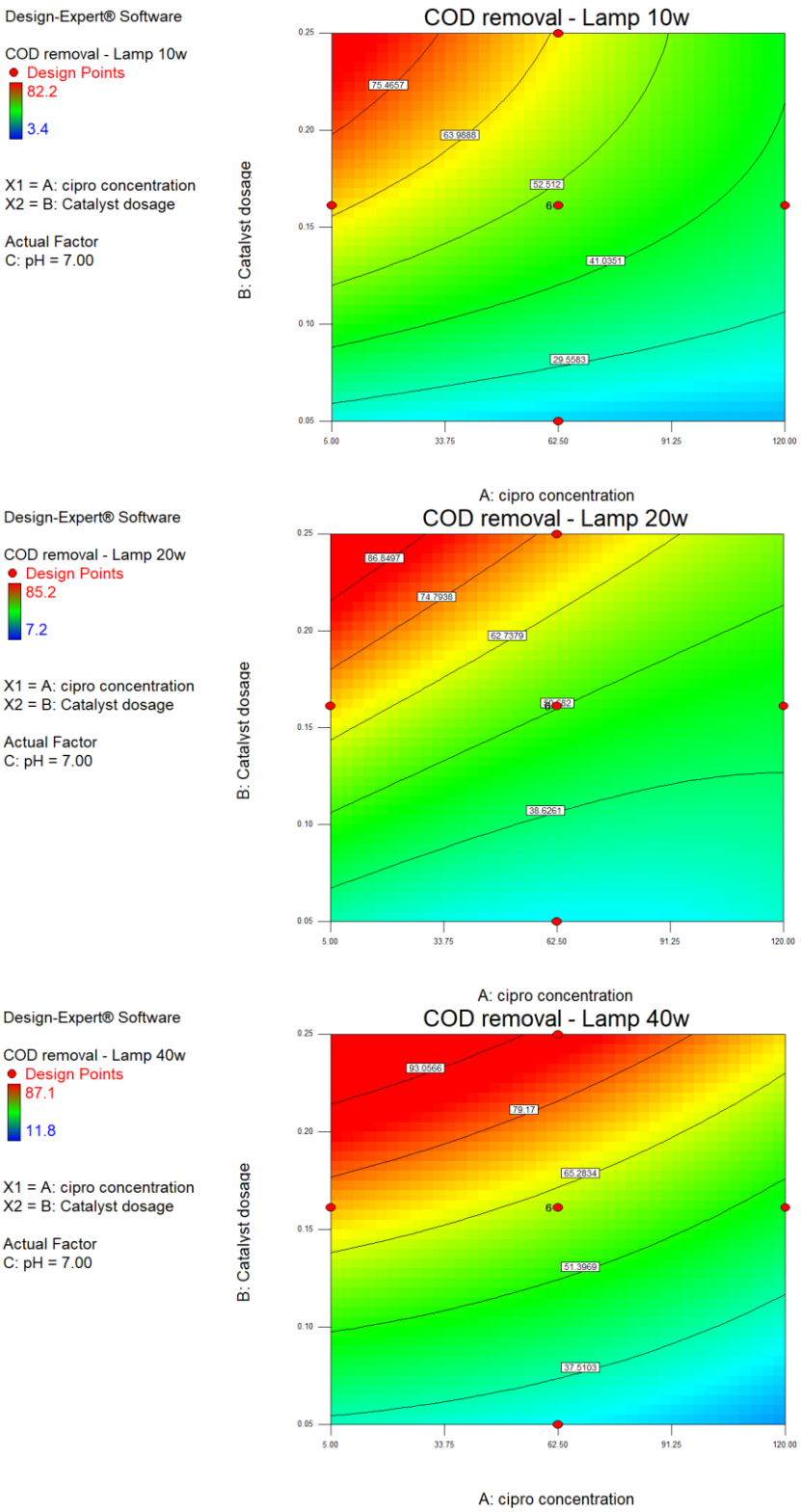

Fig. 3. Effect of CIP concentration and g-C_3N_4/Fe_3O_4 dosage on COD removal efficiency

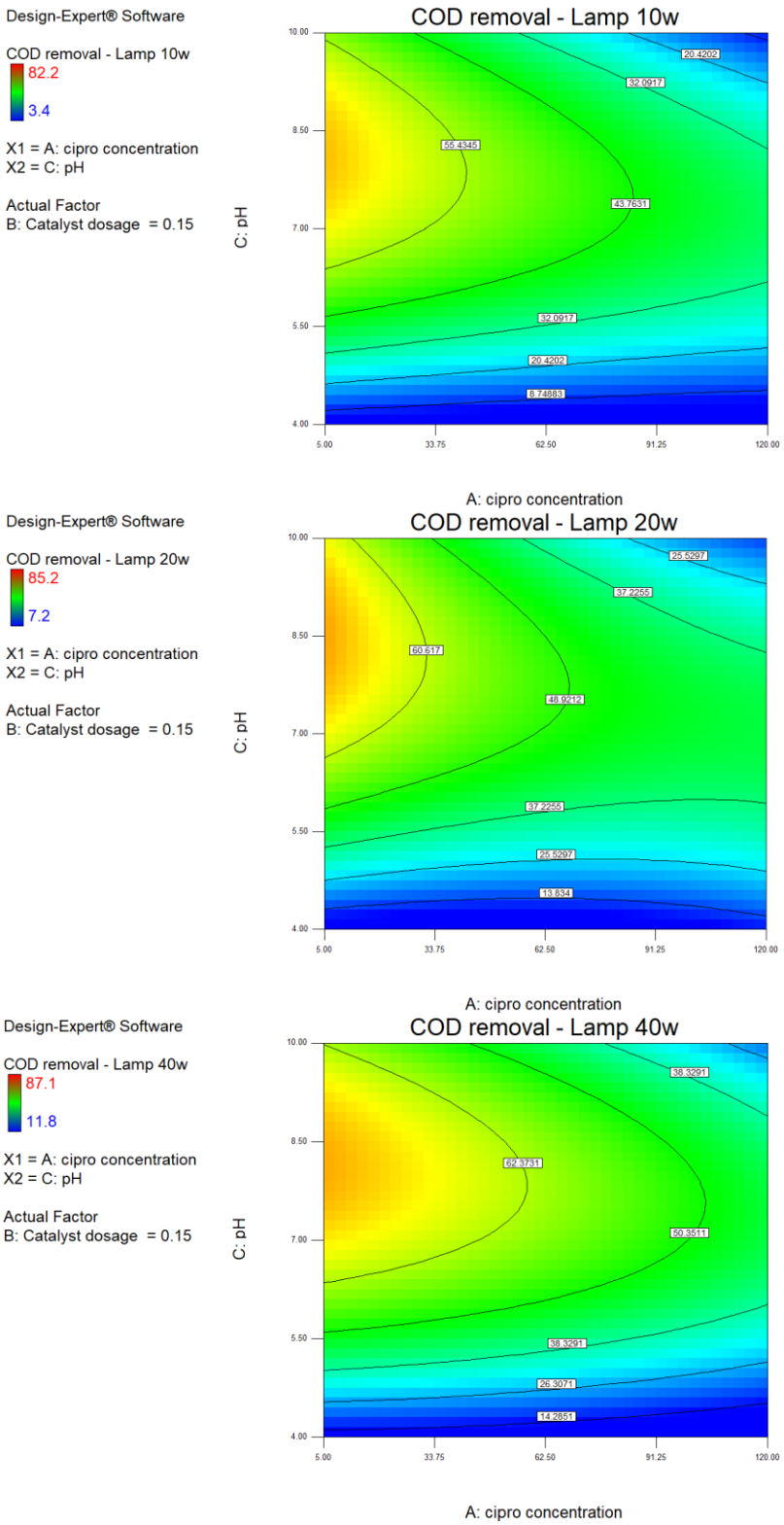

Fig. 4. Effect of CIP concentration and solution pH on COD removal efficiency

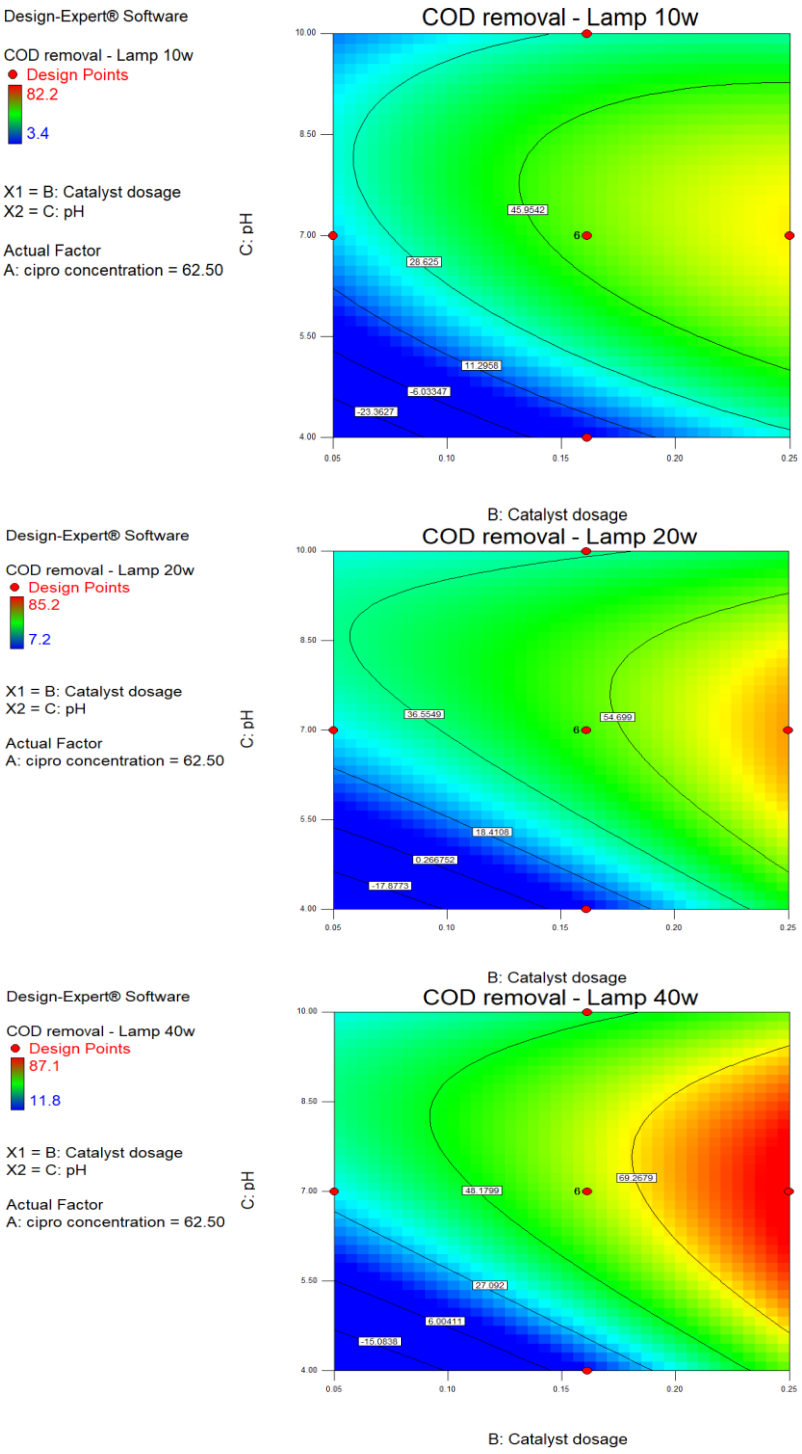

Fig. 5. Effect of g-C_3N_4/Fe_3O_4 dosage and solution pH on COD removal efficiency

Table 6. Optimization results of independent variables and corresponding predicted and experimental responses

Independent Variables			COD Removal (%)					
			Predicted			Experimental		
CIP concentration (mgL^{-1})	g-C_3N_4/Fe_3O_4 dosage (gL^{-1})	solution pH	Lamp 10 W	Lamp 20 W	Lamp 40 W	Lamp 10 W	Lamp 20 W	Lamp 40 W
8.05	0.23	7.18	82.32	90.83	98.57	82.20	85.20	87.10

Discussion

The photocatalytic performance of the magnetically recoverable g-C_3N_4/Fe_3O_4 heterostructure toward ciprofloxacin degradation under UV-C irradiation arises from the interplay between operational parameters and intrinsic material properties. Trends in COD removal efficiency with respect to catalyst dosage, initial CIP concentration, and solution pH were consistent with previous studies on g-C_3N_4-based magnetic photocatalysts [20–23], providing insight into the underlying degradation mechanisms. Among the variables studied, catalyst dosage had the most pronounced effect on COD removal. Increasing the g-C_3N_4/Fe_3O_4 loading improved photocatalytic efficiency up to an optimal point, beyond which performance declined. This non-linear behavior likely stems from excessive particle concentrations, leading to light scattering, reduced photon penetration, and partial aggregation, which limit effective catalyst activation. At optimal loadings, intimate interfacial contact between g-C_3N_4 and Fe_3O_4 facilitated efficient charge separation across the heterojunction, suppressed electron–hole recombination, and promoted ROS formation.

Higher initial ciprofloxacin concentrations negatively affected COD removal efficiency, primarily due to inner-filter effects. The aromatic and heterocyclic moieties of CIP absorb a significant portion of incident UV-C radiation, reducing photon availability for catalyst excitation. Higher pollutant loads also increase competition for ROS, further limiting degradation efficiency. Similar concentration-dependent inhibition effects have been reported for fluoroquinolone antibiotics using magnetic g-C_3N_4 composites [24–26].

Solution pH significantly influenced photocatalytic performance by altering catalyst surface charge, ciprofloxacin speciation, and interfacial interactions. Maximum COD removal occurred near neutral pH, where favorable electrostatic interactions between the catalyst surface and zwitterion or anionic CIP molecules enhanced adsorption and subsequent oxidation. Under acidic conditions, proton abundance may suppress hydroxyl radical formation, whereas strongly alkaline environments favor scavenging of reactive radicals by carbonate and bicarbonate species, collectively reducing oxidative degradation efficiency [27,28].

The observed enhancement in photocatalytic activity aligns with the principles of heterojunction engineering. Multicomponent and magnetic photocatalysts are known to improve charge separation and interfacial carrier migration. Ternary systems such as Bi_2MoO_6/g-C_3N_4/$BiFeO_3$ and magnetic composites including Fe_3O_4/Bi_2WO_6 have shown similar performance improvements due to synergistic interactions between semiconductor phases and magnetic components [29–33]. In our experiments, these mechanisms were reflected in the high COD removal efficiencies observed under optimized conditions.

The application of RSM enabled systematic evaluation of both individual and interactive effects of operational variables. Statistically significant models, supported by high R^2 values and negligible lack-of-fit, confirmed the adequacy of the RSM approach for describing process behavior within the experimental domain. These results highlight the usefulness of RSM for guiding experimental design and optimizing photocatalytic conditions efficiently [17,18].

Overall, the enhanced photocatalytic degradation of ciprofloxacin by the g-C_3N_4/Fe_3O_4 heterostructure can be ascribed to a combination of heterojunction-assisted charge separation, efficient ROS generation, and favorable interfacial interactions. The magnetic recoverability of the nanocomposite further increases its practical applicability for water treatment, highlighting that such engineered heterostructures provide a viable strategy for the removal of persistent pharmaceutical contaminants from aqueous environments.

Conclusion

The statistical analysis confirmed that the quadratic response surface models reliably describe the photocatalytic degradation of ciprofloxacin over the g-C_3N_4/Fe_3O_4 heterostructure under UV-C irradiation. The close agreement between experimental results and model predictions, reflected in coefficients of determination (R^2 = 0.837-0.882) and non-significant lack-of-fit ($p > 0.05$), confirms the validity of the models for interpreting and optimizing process performance within the studied experimental domain. ANOVA results further highlighted the significance of linear, interaction, and quadratic terms, confirming the inherently nonlinear behavior of the system.

Regression analysis identified ciprofloxacin concentration, catalyst loading, and solution pH as the primary factors controlling COD removal efficiency. Among these, g-C_3N_4/Fe_3O_4 dosage had the strongest positive linear effect, indicating the role of heterojunction-assisted charge separation and enhanced interfacial redox activity under UV-C irradiation.

A pronounced quadratic dependence on catalyst dosage indicated an optimal loading threshold at approximately 0.23 gL^{-1}; above this value, COD removal efficiency decreased due to light scattering, reduced photon penetration, and aggregation of the magnetic nanocomposite, consistent with previously reported behavior of magnetically recoverable photocatalysts.

Higher ciprofloxacin concentrations negatively affected degradation efficiency beyond the model-predicted optimum (~8.05 mgL^{-1}). At elevated concentrations, increased absorption by the

ciprofloxacin chromophore induced inner-filter effects, limiting photon availability at the catalyst surface and constraining ROS formation, consistent with previous observations in other fluoroquinolone photocatalytic systems.

Solution pH significantly influenced COD removal by modulating catalyst surface charge, ciprofloxacin speciation, and interfacial electrostatic interactions. Near-neutral pH provided optimal conditions, facilitating favorable interactions between the g-C_3N_4 framework and zwitterionic or anionic ciprofloxacin species. Acidic conditions suppressed hydroxyl radical generation, whereas strongly alkaline conditions promoted radical scavenging by carbonate species, collectively reducing oxidative degradation efficiency.

Validation experiments under optimized conditions confirmed the robustness of the RSM approach, with experimental COD removal efficiencies in close agreement with model predictions across all irradiation intensities. Overall, these findings demonstrate that the g-C_3N_4/Fe_3O_4 heterostructure is an effective UV-assisted photocatalyst for ciprofloxacin degradation, and that RSM provides a reliable framework for systematic process optimization and performance evaluation.

Disclosure Statement

No potential conflict of interest reported by the authors.

Funding

This research did not receive any specific grant from funding agencies in the public, commercial, or not-for-profit sectors.

Authors' Contributions

All authors contributed to data analysis, drafting, and revising of the paper and agreed to be responsible for all the aspects of this work.

References

[1] Kümmerer, K. (**2009**). Antibiotics in the aquatic environment A Review Part I. *Chemosphere*, 75, 417-434.

[2] Bineta, I., Kirmani, O. (**2025**). A review of g-C_3N_4-based photo catalysts for antibiotic elimination: Mechanistic insights and operational parameters. *Chinese Journal of Analytical Chemistry, in press*, 100626.

[3] Michael, I., Rizzo, L., McArdell, C. S., Manaia, C. M., Merlin, C., Schwartz, T., Dagot, C., & Fatta-Kassinos, D. (**2013**). Urban wastewater treatment plants as hotspots for the release of antibiotics in the environment: A review. *Water Research*, 47, 957-995.

[4] Dang, H. T., & Nguyen, M. V. (**2025**). Research on the synthesis, characterization, and photocatalytic activity of $BiVO_4$/g-C_3N_4 and its application in treating ciprofloxacin antibiotic in water environment. VNU Journal of Science: *Natural Sciences and Technology*.

[5] Tran, H. T. V., Nguyen, V. M., Nguyen, H. T. A., Nguyen, H. T. L., Pham, T. T., Nguyen, D. T., & Nguyen, V. N. (**2025**). Enhanced photocatalytic degradation of ciprofloxacin using a Bi_2MoO_6/g-C_3N_4 heterojunction under visible light irradiation. *Journal of Water and Environment Technology*, 23(6), 293-304.

[6] Chong, M. N., Jin, B., Chow, C. W. K., & Saint, C. (**2010**). Recent developments in photocatalytic water treatment technology: A review. *Water Research*, 44, 2997-3027.

[7] Li, K., Chen, M., Chen, L., Zhao, S., Xue, W., & Han, Y. (**2023**). Synthesis and application of a Fe_3O_4/Ag_3PO_4/g-C_3N_4 magnetic composite photo catalyst for sulfonamide antibiotics degradation. *Sustainability*, 15(17), 13279.

[8] Tang, Z., Hu, C., Zhang, R., Yu, J., Cai, L., Yang, Z., Wang, X., & Wu, S. (**2024**). Investigation of the photocatalytic activity of magnetically recoverable g-C_3N_4/$CoFe_2O_4$/Bi_2MoO_6 particles for purifying tetracycline antibiotics: Synthesis, characterization, Eco toxicity analysis, and plant toxicity test. *RSC Advances*, 14, 15302-15318.

[9] Asewuyi, A, Oderide, R. (**2024**), Graphitic carbon nitride-modified cerium ferrite for antibiotic degradation, *Journal of Materials Science: Materials in Engineering*, 19,37.

[10] Basovi, P., Selvaraj, Y., Perumal, S., et al. (**2025**). Graphitic carbon nitride (g–C3N4)–Based Z-scheme photocatalysts: Innovations for energy and environmental applications, *Materials Today Sustainability*, 29, 101069.

[11] Zhu, Z., Huo, P., Lu, Z., Yan, Y., (**2018**). Fabrication of magnetically recoverable photo catalysts using g-C_3N_4 for effective separation of charge carriers through Like-Z-scheme mechanism with Fe_3O_4 mediator. *Chemical Engineering Journal*, 331, 615-625.

[12] Shan, J., Wu, X., Li, C., et al. (**2023**). Photocatalytic degradation of tetracycline hydrochloride by a Fe3O4/g-C3N4/rGO magnetic nanocomposite mechanism: modeling and optimization, *Environ Sci Pollut Res Int.*, 30(3):8098-8109.

[13] Verma, A., Sharma, G., Wang, T., Kumar, A., Dhiman, P., & García-Peñas, A. (**2024**). Graphitic carbon nitride-based magnetic photocatalysts for removal of antibiotics. *Carbon Letters*, 35, 45-73.

[14] Mahmoudi, K., Farzadkia, M., Kalantari, R., Sobhi, H., Yeganeh, M., Esrafili, A. (**2024**). Efficient removal of ox tetracycline antibiotic from aqueous media using UV/g-C3N4/Fe3O4 photocatalytic process, *Heiliyon*, 10(9), e30604.

[15] Taravati, A., Poursattar Marjani, A., Bibak, S., et al. (**2025**). One-pot synthesis of g-C_3N_4/Fe_3O_4/CuO magnetic photo catalyst for

methylene blue degradation. *Scientific Reports*, 15, 36817.
[16] John, K., Ho, G., Li, D. (**2024**). Recent progresses in synthesis and modification of g-C3N4 for improving visible-light-driven photocatalytic degradation of antibiotics, *Water Sci Technol*, 89(11):3047-3078.
[17] Bezerra, M. A., Santelli, R. E., Oliveira, E. P., Villar, L. S., & Escaleira, L. A. (**2008**). Response surface methodology (RSM) as a tool for optimization in analytical chemistry. *Talanta*, 76, 965-977.
[18] Esfandiaribayat, M., Binazadeh, M., Sabbaghi, S., et al. (**2024**). Tetracycline removal from wastewater via g-C_3N_4-loaded RSM-CCD-optimised hybrid photocatalytic membrane reactor. *Scientific Reports*, 14, 1163.
[19] Jiao, Y., Mao, Y., Liu, Q., Ma, Y., Fu, F., Jian, S., Liu, Y., & Lu, S. (**2025**). Molten-salt-assisted preparation of g-C_3N_4 for photocatalytic degradation of tetracycline hydrochloride: Mechanism, pathway, and toxicity assessment. *Sustainability*, 17(3), 31166.
[20] Mo, C., Zhou, L., Zheng, J., & Liang, B. (**2024**). Efficient photo degradation of antibiotics by g-C_3N_4 and 3D flower-like Bi_2WO_6 perovskite structure: Insights into mechanism. *Chemosphere*, 359, 142286.
[21] Gao, X., Shan, P., Shi, W., & Guo, F. (**2025**). Photo thermal-assisted photocatalytic degradation of antibiotic by black g-C_3N_4 materials derived from C/N precursors and tetrachloro fluorescein. Catalysts, 15(5), 504.
[22] Qiao, M., Ying, G. G., Singer, A. C., & Zhu, Y. G. (**2018**). Review of antibiotic resistance in China and its environment. *Environment International*, 110, 160-172.
[23] Homem, V., & Santos, L. (**2011**). Degradation and removal methods of antibiotics from aqueous matrices A review. *Journal of Environmental Management*, 92, 2304-2347.
[24] Ma, L., Fang, Z., Duan, J., Li, J., Zhu, K., Jiang, Y., Ji, B., & Yang, Z. (**2024**). Mesoporous TiO_2@g-C_3N_4 nanostructure-enhanced photocatalytic degradation of tetracycline under full-spectrum sunlight. *Molecules*, 29(24), 5981.
[25] Le Chi, N., et al. (**2024**). Development of heterojunction C-TiO_2/g-C_3N_4 as new photocatalysts for degradation of antibiotics pollutant in aqueous environment. *VNU Journal of Science: Natural Sciences and Technology*, 41(1).
[26] Champati, A., Sahu, P. K., Rath, A., Naik, B., & Pradhan, A. (**2025**). Enhanced photo degradation of antibiotics and antimicrobial activity by a g-C_3N_4/g-C_3N_5 Nano sheet heterojunction photo catalyst. *ACS Omega*, 10(38), 43871-43890.
[27] Luo, Y., et al. (**2024**). Detection methods for antibiotics in wastewater: A review. *Bioprocess and Bio Systems Engineering*, 47, 1433-1451.
Daneshvar, N., Salari, D., & Khataee, A. R. (**2004**). Photocatalytic degradation of azo dye Acid Red 14 in water: Investigation of the effect of operational parameters. *Journal of Photochemistry and Photobiology A: Chemistry*, 157, 111-116.
[28] Zhao, Y., Li, W., & Chen, J. (**2023**). Synthesis and application of Fe_3O_4/Ag_3PO_4/g-C_3N_4 magnetic composite photo catalyst for sulfonamide antibiotics degradation. *Sustainability*, 15(17), 13279.
[29] Khyave, A. E., Mafigholami, R., Davood, A., Mahvi, A., & Salimi, L. (**2025**). Photocatalytic degradation of azithromycin and ceftriaxone using synthesized Ag/g-C_3N_4/Fe_3O_4 nanocomposites in aqueous solution. *Scientific Reports*, 15(1), 30588.
[30] Huang, C., Chen, L., Li, H., Mu, Y., & Yang, Z. (**2019**). Synthesis and application of Bi_2WO_6 photo catalysts for fluoroquinolone antibiotic degradation under visible light. *RSC Advances*, 9, 27768-27779.
[31] Li, C., Jiang, F., Sun, D., et al. (**2024**). Construction of S-scheme $Cs_3PMo_{12}O_{40}$/$MnIn_2S_4$ heterojunction for efficient photocatalytic removal of antibiotics: degradation pathways and insights. *Journal of Alloys and Compounds*, 976, 173072.
[32] Rasheed-Adeleke, A. A., Seheri, N. H., Oyewo, O. A., Makgato, S. S., Ferjani, H., & Onwudiwe, D. C. (**2025**). Enhanced photocatalytic degradation of tetracycline using Ag_3PO_4/$ZnFe_2O_4$ composite. *Applied Physics A*, 131, 857.